AGU ADVANCING EARTH AND SPACE SCIENCES

Geophysical Research Letters®

RESEARCH LETTER
10.1029/2023GL103432

Key Points:

- The lower limit of velocity change values, where reliable estimates can be derived, depends on noise characteristics of Global Navigation Satellite System time series
- Increased rift-perpendicular movement before the 2014 Bárðarbunga dike intrusion is inferred with 95% confidence, 120 km north of it
- Concurrent far-field velocity anomalies and near-field precursors may indicate coupling between distant volcanic systems at a plate boundary

Supporting Information:

Supporting Information may be found in the online version of this article.

Correspondence to:

Y. Yang,
yiy1@hi.is

Citation:

Yang, Y., Sigmundsson, F., & Geirsson, H. (2023). Joint Bayesian modeling of velocity break points, noise characteristics, and their uncertainties in GNSS time series: Far-field velocity anomalies concurrent with magmatic activity in Iceland. *Geophysical Research Letters*, *50*, e2023GL103432. https://doi.org/10.1029/2023GL103432

Received 24 MAR 2023
Accepted 29 JUN 2023

Joint Bayesian Modeling of Velocity Break Points, Noise Characteristics, and Their Uncertainties in GNSS Time Series: Far-Field Velocity Anomalies Concurrent With Magmatic Activity in Iceland

Yilin Yang[1], Freysteinn Sigmundsson[1], and Halldór Geirsson[1]

[1]Nordic Volcanological Center, Institute of Earth Sciences, University of Iceland, Reykjavík, Iceland

Abstract Estimating the timing of velocity changes (break points) in Global Navigation Satellite System (GNSS) coordinate time series is required for understanding various Earth processes and how they may couple with each other. We jointly estimate break points, noise parameters and their uncertainties in GNSS time series using Bayesian interference. Synthetic data experiments demonstrate that time-correlated noise can cause spurious estimates of break points for small velocity change and suggest the lower limits of velocity change for reliable estimates. A case study at the Krafla volcanic system shows increased rift-perpendicular movementof 7.6–9.8 mm/yr, preceding by 23–77 days the 2014 Bárðarbunga rifting episode that occurred ∼120 km to the south (maximum likelihood estimates). These far-field velocity anomalies occur in the same period as enhanced near-field seismicity and deformation before the dike intrusion at Bárðarbunga, possibly indicating the coupling between the two volcanic systems through a deep partial melt zone.

Plain Language Summary The velocity of ground movements can change due to Earth's activities. Satellite positioning techniques record these changes, while noise in the records may obscure their analyses. We developed a statistical method to detect velocity changes from these noisy records and give an estimate of uncertainty. Simulated data is used to examine the method, revealing the lower limits of velocity change for reliable estimates. Then the method is applied to detect velocity changes in the records at the Krafla volcanic system, Iceland. With maximum likelihood estimates, it is inferred that the ground moves 7.6–9.8 mm/yr faster, in rift-perpendicular direction, before the start of the 2014 Bárðarbunga dike intrusion that occurred ∼120 km to the south. The ground movements resume to approximately the original velocities by a second velocity change in late 2014 or early 2015. The onset of the far-field velocity anomalies occurs in the same period as enhanced near-field seismicity and deformation rate before the dike intrusion at Bárðarbunga. In the context of enhanced seismicity at the Bárðarbunga volcano and rapid inflation at the Askja volcano before the Krafla rifting episode in 1975–1984, our result may again indicate coupling among the volcanic systems in Iceland.

1. Introduction

Velocity changes of ground deformation, recorded with Global Navigation Satellite System (GNSS) coordinate time series, can manifest various geophysical processes, for example, volcanic-hydrothermal processes, tectonics, and the variation in groundwater level (Borsa et al., 2014; Davis et al., 2006; Geirsson et al., 2010). Break points in GNSS time series, defined as the timing of velocity changes, may signal the changes of causative processes. Together with velocity change values, they provide valuable information for many applications. In this study, a method is developed for the joint estimation of break points, velocity change values and their associated uncertainties. We applied the method to study the transient deformation in the Northern Volcanic Zone (NVZ) of Iceland during 2014–2015.

Previous studies have applied advanced methods to model velocity changes with continuous curves, for example, polynomials, wavelets, singular spectrum analysis, and Kalman filter (Borghi et al., 2012; Bos et al., 2020; Didova et al., 2016; Wang et al., 2016). However, such approach obstructs the finding of break points. In contrast, piecewise functions are transparent for estimating both break points and velocity change values (e.g., Davis et al., 2006; Ducrocq et al., 2021). Detecting break points for piecewise functions is a non-linear problem because the location of a break point affects velocity estimation.

Statistical criteria considering fitting error have been applied to detect break points for piecewise functions (Benciolini et al., 2012; Bos et al., 2018; Vitti, 2012; Wu et al., 2018). These methods usually report the optimal break points but without uncertainties. Another approach to detect break points is Bayesian modeling, with a Markov Chain Monte Carlo method, inferring the posterior distribution of parameters, and thereby obtaining parameter estimates and uncertainties jointly. This approach has been widely used in some aspects of GNSS time series analysis (Baragatti et al., 2019; Borghi et al., 2012; Koulali & Clarke, 2021; Olivare-Pulido et al., 2020; Olivares & Teferle, 2013; Qianqian & Qingming, 2013). With Bayesian modeling, Liu et al. (2023) determined the onset time of unrest at Socompa volcano, assuming white noise (WN) in GNSS time series. Oelsmann et al. (2022) detected velocity changes accompanied with steps, considering the noise as the first-order autoregressive process, or AR(1). However, more realistic noise model is required as the noise conforms to AR(1) only when sufficient signals are subtracted (Amiri-Simkooei et al., 2007), and velocity changes without simultaneous steps need further examination with the Bayesian approach.

The noise in GNSS time series is usually described using power-law noise (PLN), of which the power spectrum follows:

$$P(f) = P_0 \left(\frac{f}{f_0} \right)^{\kappa} \tag{1}$$

where $P(f)$ is the power at frequency f of the noise, P_0 and f_0 are constants, and κ is the spectral index (Williams, 2003). κ for GNSS time series ranges from -2 to 0 and is usually estimated individually for each station and coordinate component. When κ is 0, -1 and -2, the noise behaves as WN, flicker noise (FLN) and random-walk noise, respectively. PLN is caused by the complexity of signals in GNSS time series and the simplified models in data processing (Amiri-Simkooei et al., 2017; Dmitrieva et al., 2017; Dong et al., 2002; Klos et al., 2018; Langbein & Johnson, 1997; Wang & Herring, 2019; Zhou et al., 2019). Neglecting PLN oversimplifies the temporal relationship among observations in the time series and causes underestimation of uncertainties (Mao et al., 1999). Thus, the joint estimation of velocity changes and PLN parameters will enhance the reliability of results.

Therefore, we implement Bayesian modeling to jointly estimate break points, velocity change values, PLN parameters and their uncertainties. We examine the performance of the method with synthetic data and apply it to infer the timing of transient deformation in the NVZ of Iceland during 2014–2015.

2. Methods

We start with a common function model of GNSS time series. It is subsequently simplified with data pre-processing to reduce calculation cost. Then Bayesian modeling of velocity changes is implemented based on the Geodetic Bayesian Inversion Software (GBIS; Bagnardi & Hooper, 2018) using MATLAB.

A function model for a GNSS time series considering steps and velocity changes is (Nikolaidis, 2002):

$$\begin{aligned} y = {} & a + bt + \sum_{i=1}^{2} [c_i \sin(2\pi i t) + d_i \cos(2\pi i t)] \\ & + \sum_{j=1}^{m} e_j \mathrm{H}(t - t_j) + \sum_{k=1}^{n} g_k (t - t_k) \mathrm{H}(t - t_k) + \varepsilon \end{aligned} \tag{2}$$

where y is the coordinate at time t, a and b are initial station position and velocity, c_i and d_i are the amplitudes of annual and semi-annual signals, and m is the number of steps with e_j and t_j being their magnitudes and timing, respectively. n is the number of velocity changes with t_k and g_i being corresponding timing (break points) and values. H( ) is the Heaviside function. ε is residual, the difference between the observation and the model. The noise is usually assessed from residuals, of which the covariance matrix $\mathbf{C}$ is a combination of WN and PLN (Amiri-Simkooei et al., 2007; Langbein, 2012; Williams, 2003):

$$\mathbf{C} = \alpha^2 \mathbf{I} + \beta^2 \mathbf{J}_{\kappa} \tag{3}$$

here α and β represent the amplitudes of WN and PLN, respectively. $\mathbf{I}$ indicates the identity matrix and the calculation of $\mathbf{J}_{\kappa}$ is described in Text S1 in Supporting Information S1.

Pre-processing of the time series preliminarily estimates all parameters, retains the velocity changes, and removes other signals. The procedure (Table S1 in Supporting Information S1) includes: (a) removing outliers, (b) visually detecting steps and approximate break points, (c) preliminarily estimating a, b, c_i, d_i, e_j and g_k; (d) evaluating α, β, and κ from residuals, and (e) subtracting a, steps, and seasonal signals from the time series. Our pre-processing partially uses the HECTOR software (Bos et al., 2013). After pre-processing, the function model is simplified as:

$$y = a' + bt + \sum_{k=1}^{n} g_k(t - t_k)\mathrm{H}(t - t_k) + \varepsilon \quad (4)$$

where a' is the residual intercept with its value approaching zero. The data and residual vectors can be denoted as $\mathbf{y}$ and ε, respectively. By fixing WN amplitude as the estimate $\hat{\alpha}$ from pre-processing, Equation 3 is simplified as:

$$\mathbf{C} = \hat{\alpha}^2\mathbf{I} + \beta^2\mathbf{J}_\kappa \quad (5)$$

This is justified based on the relatively small effect of WN on uncertainties (Hackl et al., 2011).

We estimate the remaining parameters in Equations 4 and 5 simultaneously with Bayesian interference. The parameter vector is

$$\mathbf{m} = \left[a'\ b\ t_1 \cdots t_n\ g_1 \cdots g_n\ \kappa\ \beta\right] \quad (6)$$

where $t_1 \cdots t_n$ represent break points and $g_1 \cdots g_n$ represent velocity change values. The joint conditional probability distribution (PD) of $\mathbf{m}$ given observations $\mathbf{y}$ can be derived with Bayesian theorem:

$$\mathrm{p}(\mathbf{m}|\mathbf{y}) = \frac{\mathrm{p}(\mathbf{y}|\mathbf{m})\mathrm{p}(\mathbf{m})}{\mathrm{p}(\mathbf{y})} \quad (7)$$

where $\mathrm{p}(\mathbf{m}|\mathbf{y})$ is the targeted PD and $\mathrm{p}(\mathbf{y}|\mathbf{m})$ indicates the PD of $\mathbf{y}$ given $\mathbf{m}$. $\mathrm{P}(\mathbf{m})$ is the a priori PD of $\mathbf{m}$, which we assume to follow uniform distribution within the search range of $\mathbf{m}$. The search range is set according to the pre-processing results. The logarithm of $\mathrm{p}(\mathbf{y}|\mathbf{m})$ can be calculated assuming Gaussian distribution of the parameters (Koulali & Clarke, 2021; Langbein, 2004):

$$\ln(\mathrm{p}(\mathbf{y}|\mathbf{m})) = -\frac{1}{2}\left(N\ln(2\pi) + \ln(\det(\mathbf{C})) + \varepsilon^{\mathrm{T}}\mathbf{C}^{-1}\varepsilon\right) \quad (8)$$

where N is the number of data points. Iterated sampling of $\mathbf{m}$ with Metropolis-Hastings algorithm (Bagnardi & Hooper, 2018; Hastings, 1970; Metropolis et al., 1953) gives an estimate of the posterior joint distribution of parameters, denoted as $\hat{\mathrm{p}}(\mathbf{m}|\mathbf{y})$. With $\hat{\mathrm{p}}(\mathbf{m}|\mathbf{y})$, one has all statistical information of the parameter estimates, including a parameter combination with the maximum likelihood (denoted as the optimal estimates) and the individual mean values of the marginal PDs (denoted as the mean estimates). The 95% confidence interval of $\hat{\mathrm{p}}(\mathbf{m}|\mathbf{y})$ is denoted as uncertainty hereinafter.

3. The Validation of Bayesian Modeling With Synthetic Time Series

We validate the method with synthetic time series generated with Equation 4 and pre-processing results of observed data (Table S2 in Supporting Information S1). For clearer comparison of the results, we added WN and FLN. The WN amplitude is set to 1 mm, and the FLN amplitude varies among 3, 4, and 5 mm/yr$^{0.25}$. The time series spans 5 yr, from 2019 to 2024. The initial velocity is 5 mm/yr, and one break point is simulated at the middle of the time series (2.5 yr). The velocity change is set to −1.0, −2.5, −5.0, −7.5, −10.0, −15.0, −20.0 mm/yr. Pre-processing follows Section 2, but the seasonal signals are not estimated nor removed. The preliminary estimate of break point is set to 2.55 yr. We run 120,000 sampling iterations for the synthetic series. The search range of the parameters is in Table S3 in Supporting Information S1 and the synthetic time series are displayed in Figure S1 in Supporting Information S1.

Figures 1a–1c show the synthetic data and inferred models. For g of −20 mm/yr (Figure 1a), the model fits the time series well, with the estimation error of break point smaller than 10 d and its uncertainty of 60 d, illustrating the effectiveness of the method. For g of −5 mm/yr (Figure 1b), the simulated break point is masked by the noise. The estimation error is larger than 1 yr, although the 95% confidence interval includes the true break point. Thus,

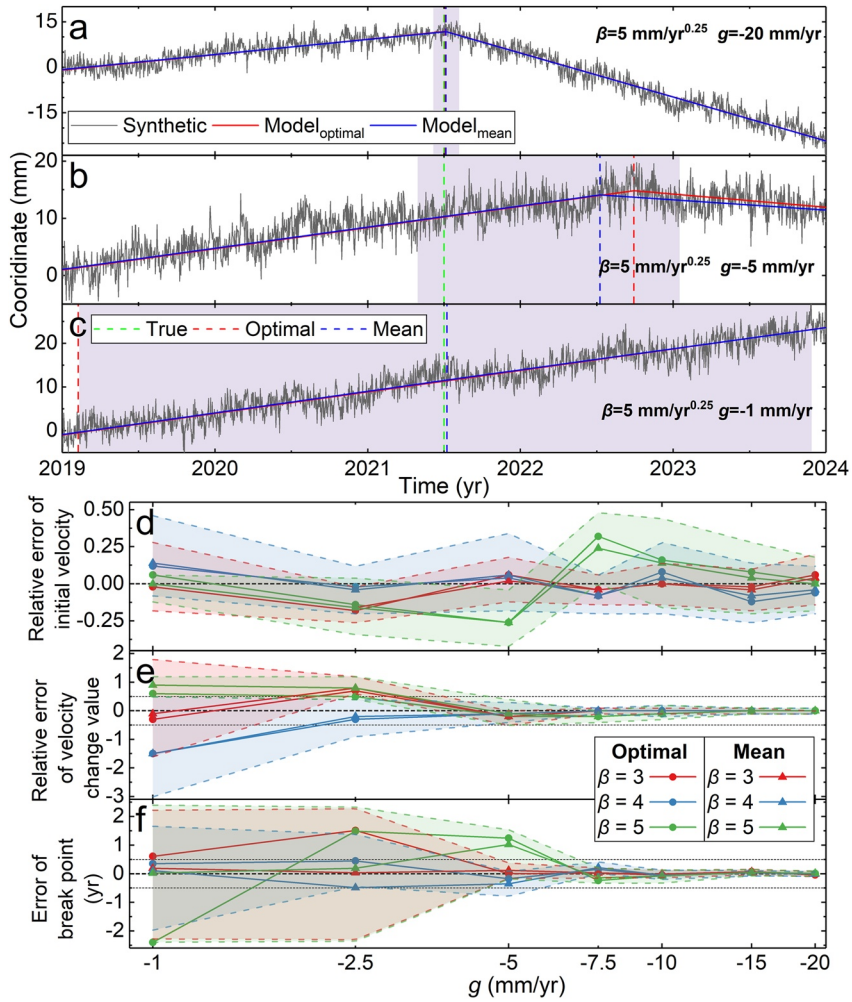

Figure 1. Synthetic data experiments with a single break point, different noise levels and velocity change values. (a–c) Synthetic time series and the established models with FLN amplitude (β) of 5 mm/yr$^{0.25}$ and velocity changes (g) of −20, −5, and −1 mm/yr, respectively. The purple shaded area indicates the 95% confidence interval of break points. (d–f) The estimation errors and uncertainties of synthetic experiments. The relative errors are the differences between the estimates and true values, divided by the true values. The horizontal axes are with a logarithmic scale.

the estimates of break points with small velocity changes can be offset by PLN. g of −1 mm/yr yields break point uncertainty similar to the search range. In this case the Markov chain (Figure S2 in Supporting Information S1) fails to converge, inducing random values within the search range taken as an estimate, which should not be accepted. We study the general variations of estimation for different g, aiming at break point uncertainty smaller than half a year (Figures 1d–1f and Table S4 in Supporting Information S1). In a 5-yr-length time series, we suggest the velocity change value be larger than −7.5, −10, and −15 mm/yr for FLN amplitude of 3, 4, and 5 mm/yr$^{0.25}$ for a reliable break point estimate.

The temporal characteristics of individual noise series can vary notably even with the same parameters. We do run the experiments again with another set of noise (Figure S3 in Supporting Information S1) and derive the same lower limits as above.

4. Far-Field Velocity Anomalies Concurrent With Magma Unrest

4.1. Northern Volcanic Zone of Iceland

The NVZ is a part of the Mid-Atlantic plate boundary in Iceland (Einarsson, 2008). It is divided into several volcanic systems, including Þeistareykir, Krafla, Fremrinámar, Askja and Bárðarbunga (Figure 2). Relatively

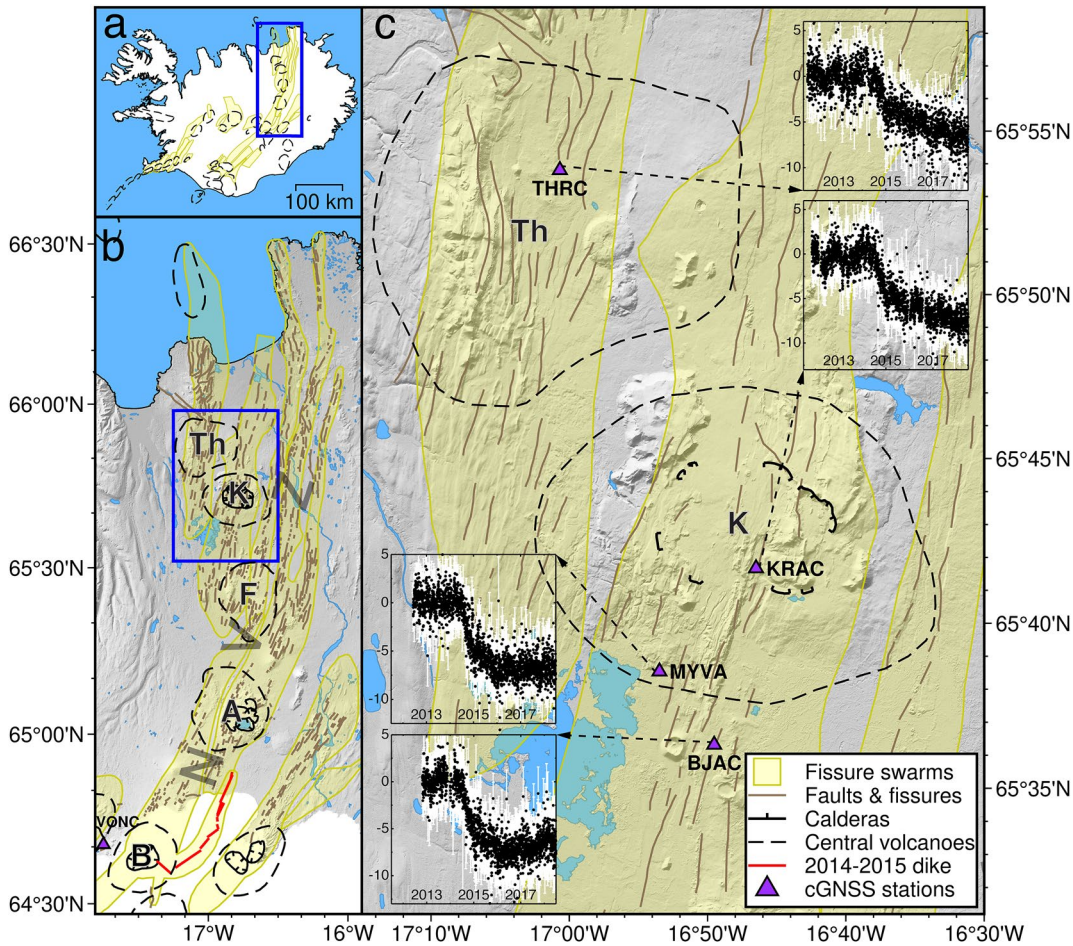

Figure 2. (a) A map of Iceland with the blue rectangle indicating the Northern Volcanic Zone (NVZ). (b) A map of NVZ with volcanic systems: B: Bárðarbunga. A: Askja. F: Fremrinámar. K: Krafla. Th: Þeistareykir (Saemundsson, 1979; Sigmundsson, Einarsson, et al., 2020). Faults and fissures swarms (brown) are from Jóhannesson and Sæmundsson (2009). Blue rectangle indicates the area shown in panel c. (c) Locations of cGNSS stations with their detrended east-component time series. The dashed lines with arrows point from the stations to their time series, where the black dots and white lines indicate the coordinates and their uncertainties, respectively (unit: mm), and the horizontal axes indicate time (unit: yr).

homogeneous mantle, consistent mantle forming conditions and similar melt fractions along the NVZ compared to the whole Iceland have been inferred with radiogenic isotopes (Harðardóttir et al., 2022). The latest rifting episode at Krafla during 1975–1984 included ~20 dike intrusions and nine eruptions, with earthquakes, faulting and accumulated widening of 4–5 m on average in the volcanic system (e.g., Björnsson et al., 1977; Wright et al., 2012). Since late 2011, ground deformation has been monitored with continuous GNSS (cGNSS) stations KRAC, MYVA and BJAC at Krafla, and THRC at Þeistareykir. In August 2014, a dike intrusion occurred at Bárðarbunga, ~120 km south of the Krafla area (Parks et al., 2017; Sigmundsson et al., 2014), which propagated 48 km and fed the 6-month-long Holuhraun eruption at its northern end. At a similar period, four cGNSS stations at Krafla and Þeistareykir show faster movements to the west (Figure 2c and Figure S4 in Supporting Information S1; Lanzi et al., 2023).

4.2. Bayesian Modeling Results

The daily coordinate time series at the four stations were derived with GAMIT/GLOBK 10.75 (Figure S4 and Text S2 in Supporting Information S1; Herring et al., 2018). Pre-processing infers velocity anomalies characterized by two break points during 2014–2015 (Figure 3 and Table S2 in Supporting Information S1). Bayesian modeling is only implemented to the east component as only its velocity changes allow reliable estimates (8 mm/yr vs. the FLN amplitude of 3.0–3.4 mm/yr$^{0.25}$ from pre-processing). We run 500,000 sampling iterations to better realize the PDs.

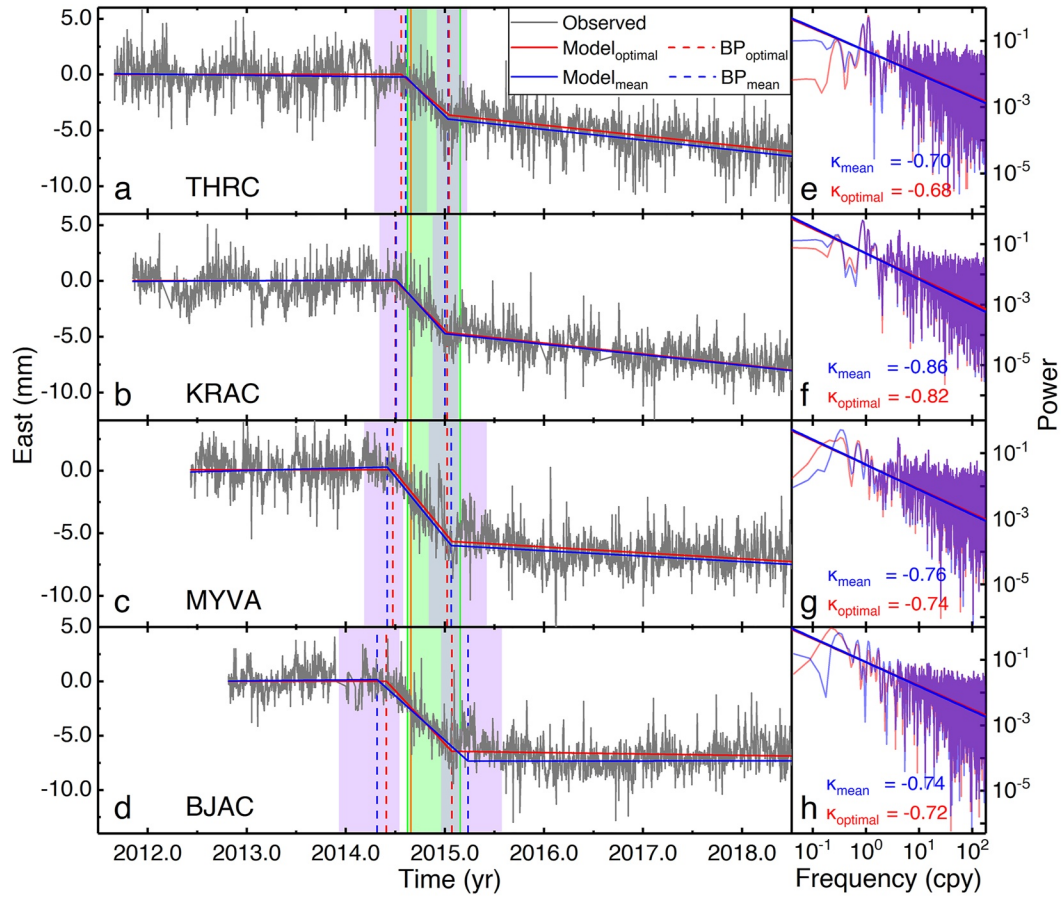

Figure 3. Bayesian modeling results for the four time series at Krafla and Þeistareykir. (a–d) Preprocessed time series in east component with the established models. The time series are detrended with the optimal initial velocities. The purple shaded area indicates the 95% confidence interval of break points. The green shaded area indicates the period of the Bárðarbunga diking and eruption (Sigmundsson et al., 2014), with the start of dike intrusion on 16 August 2014 (2014.6260) and the end of eruption on 27 February 2015 (2015.1603). The vertical orange line indicates the start of the eruption on 29 August 2014 (2014.6575). (e–h) The power spectrums of residuals and the obtained spectrum indices (κ).

Results are shown in Figures 3 and 4a, Figures S5, S6, and Table S5 in Supporting Information S1. Generally, the established models fit the time series well. For the first velocity change, the optimal estimates derive break points at 2014.4114, 2014.4758, 2014.5018, and 2014.5601 at station BJAC, MYVA, KRAC and THRC, respectively. Corresponding velocity change values are −9.8, −9.6, −8.9, and −7.6 mm/yr. The largest break point uncertainty is 227 d at BJAC, which is mainly caused by missing data, and the smallest is 102 d at KRAC. Accounting for all the stations at Krafla, the 95% confidence interval of the break points ranges from 2014.1860 to 2014.6166 (9 March to 14 August 2014). The second velocity changes have similar magnitude as the first ones, however with opposite sign. The root mean square of the differences between their absolute values is 0.7 mm/yr. The uncertainties of the second break points all overlap with the end of the Holuhraun eruption (29 August 2014).

Therefore, we infer that the westward-accelerated movements at Krafla (9 March to 14 August 2014) precede the Bárðarbunga dike intrusion (16 August 2014) with 95% confidence interval (±83 d on average). At the second break points the station velocities resume similar velocities as before the movement anomalies. The optimal estimates suggest the resumption occurs before the end of Holuhraun eruption but uncertainties allow no solid conclusion.

5. Discussion

The span of the time series affects the parameter estimations. Additional synthetic data experiments (Text S3 and Figure S7 in Supporting Information S1) indicate longer span before a break point generally reduces the uncertainties of the initial velocity and break point but has less effect on errors. For a fixed span of time series, shorter

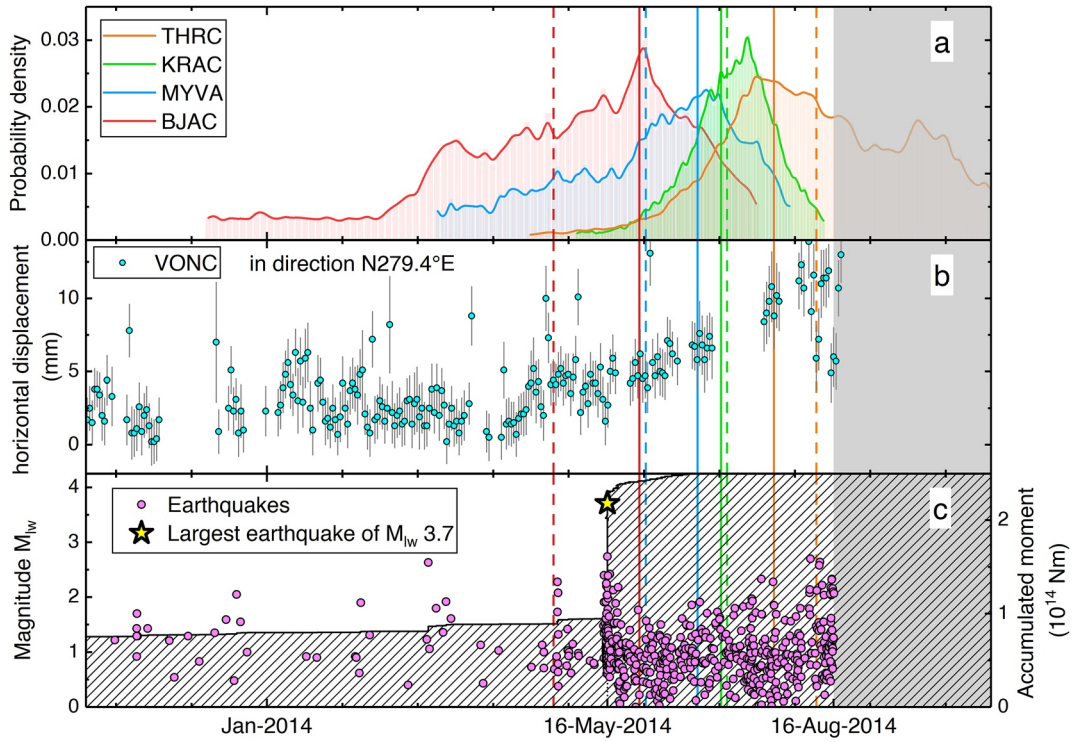

Figure 4. Comparison between the far-field velocity anomalies and near-field precursors of the Bárðarbunga rifting episode. (a) Marginal posterior probability distributions of the first break points within 95% confidence intervals. The color-shaded areas start and end at the lower and higher limit of the 95% confidence intervals, respectively. The vertical solid and dashed lines indicate the optimal and mean estimates, respectively. The gray area indicates the period after the onset of the Bárðarbunga dike intrusion. (b) The horizontal displacement in direction N279.4°E (the azimuth of maximum horizontal motion) at VONC station (11 km west of the Bárðarbunga) from detrended GNSS time series. (c) Seismicity at Bárðarbunga versus time (left axis) and accumulated seismic moment (right axis) before the dike intrusion. The data in panels b and c are from Sigmundsson, Pinel, et al. (2020).

span before the break point hampers the precision of the initial velocity while shorter span after the break point hinders the velocity change estimation. Consequently, they both raise the uncertainty of velocity change. The relatively large uncertainties of the second break points at Krafla are partially attributed to the short span (less than 1 year) between the two break points (Figure 3). The difference in the total time span of the four cGNSS time series is less than 1 yr, with minimal influence on the results.

The joint parameter distributions (Figure S6 in Supporting Information S1) indicate strong anti-correlation between the two velocity change values, and between the two noise parameters. The anti-correlation between the velocity change values is because the second one is referenced to the first one. The anti-correlation of noise parameters has been observed in previous research (e.g., Chen et al., 2018; Gobron et al., 2021). The unit of PLN amplitude varies with the spectral index in Equation 1, making their amplitudes not directly comparable. Thus, we compare the PDs of noise amplitude with the preliminary results after unit normalization (Gobron et al., 2021; Text S5 and Figure S8 in Supporting Information S1) and find that the preliminary estimates of noise amplitude are within 95% confidence intervals of Bayesian results, validating the method on noise assessment.

Magmatic processes can cause gradual velocity changes, for example, exponential-logarithmic functions (Bevis & Brown, 2014), instead of sudden changes at specific epochs as modeled in Equation 2. Our method can be generalized with different functions. However, when applying Equation 2 to gradual velocity changes, the break point uncertainty can be expected to provide an estimate of the duration of the varying velocity.

Near-field precursors prior to the onset of the Bárðarbunga dike include enhanced ground deformation and seismicity (Sigmundsson, Pinel, et al., 2020), which can be compared with the velocity anomalies at Krafla (Figure 4). The probability density of the beginning of far-field velocity anomalies is higher in the period when the near-field station, VONC (Figure 2b), moves faster away from the Bárðarbunga caldera (Figure 4b) and when

an M_{lw} 3.7 earthquake occurs at Bárðarbunga (Figure 4c), marking a period of increased seismicity lasting until the diking onset. A comparable velocity anomaly is observed at another near-field station before the dike intrusion (Figure S9b in Supporting Information S1). Therefore, the far-field velocity anomalies at Krafla occur in the same period as the near-field precursors at Bárðarbunga. These far-field velocity anomalies localize at the NVZ as the time series at other four far-field cGNSS stations at distances of 110–150 km from Bárðarbunga show no similar pattern of deformation (Figure S9c in Supporting Information S1).

The concurrent activities at Krafla and Bárðarbunga may indicate a coupling relationship between the two volcanic systems along the NVZ. During 25 October 2013–31 October 2014, five minor seismic swarms are clustered in the Krafla region (Blanck et al., 2014). Three correlate with reduced reinjection rate at two geothermal boreholes and two occur in areas of previous seismicity in 2009–2012 relating to the rift axis activities (Schuler et al., 2016). Thus, these seismic swarms cannot be taken as unusual activity relating to the velocity anomalies. The absence of unusual seismicity with the velocity anomalies may indicate the involvement of ductile processes, aseismic faulting, or insufficient strain change to cause seismicity.

Volcanic systems at NVZ may be coupled, eventually through a partial melt zone that can channel pressure variations. Pressure pulse propagation in a partial melt zone has been suggested in the past to cause coupled activity at volcanoes in the NVZ. Leveling and lake level measurements at Askja indicate rapid inflation of >20 cm/yr during 1970–1972 above a pressurized magma source, which reverses to deflation probably after 1974 (Tryggvason, 1989). At the Bárðarbunga volcano, the onset of long-lasting sequence of M5-5.5 earthquakes in 1974, signifying pressure changes in its roots, was concurrent with the magma inflow at Krafla (Einarsson, 1987, 1991). Suggested explanation was that magma flow into the roots of the Krafla volcano reduced the pressure under Bárðarbunga and Askja, causing deflation at both. The partial melt zone in the NVZ is described as a magmatic axis by Marquart and Jacoby (1985) and Jocoby et al. (1989). We envision no material flow between volcanic systems below the brittle-ductile boundary, only mechanical coupling.

Possibilities for further examination of the geodetic signals at the cGNSS sites studied here are limited, but campaign GNSS and Interferometric Synthetic Aperture Radar (InSAR) observations (Drouin et al., 2017) provide some constraints. The campaign GNSS stations nearest to the continuous ones, measured yearly, show general decrease in eastward movement consistent with cGNSS results, while the InSAR times series analysis at ground pixels close to the cGNSS stations are less conclusive (Figure S10 in Supporting Information S1).

A few studies have addressed the coupling between volcanoes and/or magma bodies. Lower crust earthquakes at 12–25 km depth at Askja during 2005–2010 implies melt injected by multiple pulses from a deep magma source (Key et al., 2011). Deep magma bodies may offset from shallow ones within the same volcanic system (Cordell et al., 2018), for example, earthquakes at 7–22 km depth and ∼12 km southeast of the Bárðarbunga caldera before the dike intrusion in 2014 can indicate a laterally offset magma feeding source (Hudson et al., 2017). At the Grímsvötn volcano, ∼27 km southeast of Bárðarbunga, velocity anomalies of ground deformation are observed ten months before the 2014 Bárðarbunga diking, indicating the decrease of magma inflow (Bato et al., 2018). Biggs et al. (2016) summarizes possible mechanisms for the coupling between volcanoes, where Campi Flegrei and Vesuvius in Italy and Mauna Loa and Kīlauea in Hawaii are also suggested to be linked with an asthenospheric source. However, the distances between these interacted volcanoes are only 25–35 km. Our finding suggests coupling over ∼120 km distance, eventually related to the mantle plume under Iceland. Future research on the spatial evolution of the velocity anomalies (e.g., with a dense cGNSS network) may provide better insight into the causative processes of long-distance volcano coupling.

6. Conclusions

Bayesian modeling is implemented to jointly estimate velocity break points, velocity change values and power-law noise in GNSS time series, together with their probability density distributions. Synthetic data experiments validate the method and suggest velocity change value exceeding 7.5, 10, and 15 mm/yr for flicker noise amplitude of 3, 4, and 5 mm/yr$^{0.25}$, respectively, can be satisfactorily detected in 5-yr-length time series. Applying the method to observed data during 2014–2015 at Krafla and Þeistareykir, we infer that a velocity change in the east component at Krafla precedes the 2014 Bárðarbunga dike intrusion by 23–77 days, with a 95% confidence level of ±83 d on average. The amount of the velocity changes is 7.6–9.8 mm/yr and the velocities resume to approximately the original level with another velocity change in late 2014 or early 2015. The onset of the velocity

anomalies occurs in the same period as enhanced seismicity and deformation rate before the dike intrusion at Bárðarbunga, possible providing evidence for large-scale coupling among the volcanic systems in the Northern Volcanic Zone of Iceland.

Data Availability Statement

The coordinate time series at the four stations are available at https://doi.org/10.17605/OSF.IO/4JDHV. The modified GBIS scripts for detecting break points in time series (GBIS4TS) are available at https://doi.org/10.17605/OSF.IO/Q35TW with a synthetic time series for verifying installation provided. The original version of the GBIS software is available at https://comet.nerc.ac.uk/gbis/ and the HECTOR software is available at http://segal.ubi.pt/web-services/whatishector/.

Acknowledgments
The authors are grateful to Nico Fournier and an anonymous referee for their important comments. This study received funding from the European Union's Horizon 2020 research and innovation programme No. 858092 (IMPROVE project) and partially from Icelandic Research Fund No. 239615-051 (ISVOLC project). We acknowledge Marco Bagnardi and Andrew Hooper (AH) for GBIS software, and AH for discussions. We thank Chiara Lanzi and Sigrún Hreinsdóttir for supporting GNSS data processing. The cGNSS stations are operated jointly with the National Power Company of Iceland. We thank Vincent Drouin for providing InSAR time series and discussions. We thank Páll Einarsson, Juliet Biggs, Fei Liu, Sæmundur A. Halldórsson, Tim J. Craig, John Maclennan, Joachim Gottsmann, Sonja Greiner, Patricia Fehrentz, Xiaohui Zhou, Yifang Ma and Alberto Caracciolo for discussions. We acknowledge International GNSS Services for data support and Space & Earth Geodetic Analysis Laboratory, Portugal, for HECTOR software. The maps are plotted with the Generic Mapping Tools (Wessel et al., 2019).

References

Amiri-Simkooei, A. R., Mohammadloo, T. H., & Argus, D. F. (2017). Multivariate analysis of GPS position time series of JPL second reprocessing campaign. *Journal of Geodesy*, *91*(6), 685–704. https://doi.org/10.1007/s00190-016-0991-9

Amiri-Simkooei, A. R., Tiberius, C. C. J. M., & Teunissen, P. J. G. (2007). Assessment of noise in GPS coordinate time series: Methodology and results. *Journal of Geophysical Research*, *112*(B7), B07413. https://doi.org/10.1029/2006JB004913

Bagnardi, M., & Hooper, A. (2018). Inversion of surface deformation data for rapid estimates of source parameters and uncertainties: A Bayesian approach. *Geochemistry, Geophysics, Geosystems*, *19*(7), 2194–2211. https://doi.org/10.1029/2018GC007585

Baragatti, M., Bertin, K., Lebarbier, E., & Meza, C. (2019). A Bayesian approach for the segmentation of series with a functional effect. *Statistical Modelling*, *19*(2), 194–220. https://doi.org/10.1177/1471082X18755539

Bato, M. G., Pinel, V., Yan, Y., Jouanne, F., & Vandemeulebrouckm, J. (2018). Possible deep connection between volcanic systems evidenced by sequential assimilation of geodetic data. *Scientific Reports*, *8*(1), 11702. https://doi.org/10.1038/s41598-018-29811-x

Benciolini, B., Reguzzoni, M., Venuti, G., & Vitti, A. (2012). Bayesian and variational methods for discontinuity detection: Theory overview and performance comparison. In N. Sneeuw, P. Novák, M. Crespi, &, F. Sansò (Eds.), *VII Hotine-Marussi Symposium on Mathematical Geodesy*. Springer.

Bevis, M., & Brown, A. (2014). Trajectory models and reference frames for crustal motion geodesy. *Journal of Geodesy*, *88*(3), 283–311. https://doi.org/10.1007/s00190-013-0685-5

Biggs, J., Robertson, E., & Cashman, K. (2016). The lateral extent of volcanic interactions during unrest and eruption. *Nature Geoscience*, *9*(4), 301–311. https://doi.org/10.1038/ngeo2658

Björnsson, A., Saemundsson, K., Einarsson, P., Tryggvason, E., & Grönvold, K. (1977). Current rifting episode in north Iceland. *Nature*, *266*(5600), 318–323. https://doi.org/10.1038/266318a0

Blanck, H., Ágústsson, K., & Gunnarsson, K. (2014). Seismic monitoring of Krafla. For the period October 2013 to October 2014. Retrieved from http://gogn.lv.is/files/2014/2014-136.pdf

Borghi, A., Cannizzaro, L., & Vitti, A. (2012). Advanced techniques for discontinuity detection in GNSS coordinate time-series. An Italian case study. In S. Kenyon, M. Pacino, & U. Marti (Eds.), *Geodesy for Planet Earth*. Springer.

Borsa, A. A., Agnew, D. C., & Cayan, D. R. (2014). Ongoing drought-induced uplift in the western United States. *Science*, *345*(6204), 1587–1590. https://doi.org/10.1126/science.1260279

Bos, M. S., Fernandes, R. M. S., & Karegar, M. (2018). The effect of colored noise on automatic offset detection in GNSS time series. In *Abstract presented at international GNSS service Wuhan workshop 2018*. Retrieved from http://acc.igs.org/workshop2018.html

Bos, M. S., Fernandes, R. M. S., Montillet, J. P., & Williams, S. D. P. (2020). Introduction to geodetic time series analysis. In J. P. Montillet & M. Bos (Eds.), *Geodetic time series analysis in Earth sciences*. Springer.

Bos, M. S., Fernandes, R. M. S., Williams, S. D. P., & Bastos, L. (2013). Fast error analysis of continuous GNSS observations with missing data. *Journal of Geodesy*, *87*(4), 351–360. https://doi.org/10.1007/s00190-012-0605-0

Chen, G., Zhao, Q., Wei, N., & Liu, J. (2018). Impacts on noise analyses of GNSS position time series caused by seasonal signal, weight matrix, offset, and helmert transformation parameters. *Remote Sensing*, *10*, 1584. https://doi.org/10.3390/rs10101584

Cordell, D., Unsworth, M. J., & Díaz, D. (2018). Imaging the Laguna del Maule volcanic field, central Chile using magnetotellurics: Evidence for crustal melt regions laterally-offset from surface vents and lava flows. *Earth and Planetary Science Letters*, *488*, 168–180. https://doi.org/10.1016/j.epsl.2018.01.007

Davis, J. L., Wernicke, B. P., Bisnath, S., Niemi, N. A., & Elósegui, P. (2006). Subcontinental-scale crustal velocity changes along the Pacific-North America plate boundary. *Nature*, *441*(29), 1131–1134. https://doi.org/10.1038/nature04781

Didova, O., Gunter, B., Riva, R., & Roese-Koerner, L. (2016). An approach for estimating time-variable rates from geodetic time series. *Journal of Geodesy*, *90*(11), 1207–1221. https://doi.org/10.1007/s00190-016-0918-5

Dmitrieva, K., Segall, P., & Bradley, A. M. (2017). Effects of linear trends on estimation of noise in GNSS position time-series. *Geophysical Journal International*, *208*(1), 281–288. https://doi.org/10.1093/gji/ggw391

Dong, D., Fang, P., Bock, Y., Cheng, M. K., & Miyazaki, S. (2002). Anatomy of apparent seasonal variations from GPS-derived site position time series. *Journal of Geophysical Research*, *107*(B4), ETG9-1.–ETG9-16. https://doi.org/10.1029/2001JB000573

Drouin, V., Sigmundsson, F., Verhagen, S., Ófeigsson, B. G., Spaans, K., & Hreinsdóttir, S. (2017). Deformation at Krafla and Bjarnarflag geothermal areas, northern volcanic zone of Iceland, 1993–2015. *Journal of Volcanology and Geothermal Research*, *344*, 92–105. https://doi.org/10.1016/j.jvolgeores.2017.06.013

Ducrocq, C., Geirsson, H., Árnadóttir, T., Juncu, D., Drouin, V., Gunnarsson, G., et al. (2021). Inflation-deflation episodes in the Hengill and Hrómundartindur volcanic complexes, SW Iceland. *Frontiers in Earth Science*, *9*, 725109. https://doi.org/10.3389/feart.2021.725109

Einarsson, P. (1987). The anomalous mantle beneath Iceland and possible pressure connection between volcanoes. In *Abstract presented at symposium on how volcanoes work*. Hilo.

Einarsson, P. (1991). Earthquakes and present-day tectonism in Iceland. *Tectonophysics*, *189*(1–4), 261–279. https://doi.org/10.1016/0040-1951(91)90501-I

Einarsson, P. (2008). Plate boundaries, rifts and transforms in Iceland. *Jökull*, *58*(12), 35–58. https://doi.org/10.33799/jokull2008.58.035

Geirsson, H., Árnadóttir, T., Hreinsdóttir, S., Decriem, J., Lafemina, P. C., Jónsson, S., et al. (2010). Overview of results from continuous GPS observations in Iceland from 1995 to 2010. *Jökull*, *2010*(60), 3–22. https://doi.org/10.33799/jokull2010.60.003

Gobron, K., Rebischung, P., Van Camp, M., Demoulin, A., & de Viron, O. (2021). Influence of aperiodic non-tidal atmospheric and oceanic loading deformations on the stochastic properties of global GNSS vertical land motion time series. *Journal of Geophysical Research: Solid Earth*, *126*(9), e2021JB022370. https://doi.org/10.1029/2021JB022370

Hackl, M., Malservisi, R., Hugentobler, U., & Wonnacott, R. (2011). Estimation of velocity uncertainties from GPS time series: Examples from the analysis of the South African TrigNet network. *Journal of Geophysical Research*, *116*(B11), B11404. https://doi.org/10.1029/2010JB008142

Harðardóttir, S., Mattews, S., Halldórsson, S. A., & Jackson, M. G. (2022). Spatial distribution and geochemical characterization of Icelandic mantle end-members: Implications for plume geometry and melting processes. *Chemical Geology*, *604*, 120930. https://doi.org/10.1016/j.chemgeo.2022.120930

Hastings, W. K. (1970). Monte Carlo sampling methods using Markov chains and their applications. *Biometrika*, *57*(1), 97–109. https://doi.org/10.1093/biomet/57.1.97

Herring, T. A., King, R. W., Floyd, M. A., & McClusky, S. C. (2018). *Introduction to GAMIT/GLOBK*. Massachusetts Institute of Technology. Retrieved from http://geoweb.mit.edu/gg/Intro_GG.pdf

Hudson, T. S., White, R. S., Greenfield, T., Ágústsdóttir, T., Brisbourne, A., & Green, R. G. (2017). Deep crustal melt plumbing of Bárðarbunga volcano, Iceland. *Geophysical Research Letters*, *44*(17), 8785–8794. https://doi.org/10.1002/2017GL074749

Jocoby, W. R., Zdarsky, H., & Altmann, U. (1989). Geodetic and geophysical evidence for magma movement and dyke injection during the Krafla rifting episode in North Iceland. In (Ed.), J. M. Sinton (Ed.), *Evolution of mid ocean ridges*. https://doi.org/10.1029/GM057p0065

Jóhannesson, H., & Sæmundsson, K. (2009). Geological map of Iceland - Tectonics - 1:600.000 [Dataset]. Icelandic Institute of Natural History. https://gatt.lmi.is/geonetwork/srv/eng/catalog.search#/metadata/%7B005FFDAD-69A1-4385-B16F-FD31B960FE33%7D/formatters/xsl-view?root=div&view=advanced

Key, J., White, R. S., Soosalu, H., & Jakobsdóttir, S. S. (2011). Multiple melt injection along a spreading segment at Askja, Iceland. *Geophysical Research Letters*, *38*(5), L05301. https://doi.org/10.1029/2010GL046264

Klos, A., Bos, M. S., & Bogusz, J. (2018). Detecting time-varying seasonal signal in GPS position time series with different noise levels. *GPS Solutions*, *22*(1), 21. https://doi.org/10.1007/s10291-017-0686-6

Koulali, A., & Clarke, P. J. (2021). Modelling quasi-periodic signals in geodetic time-series using Gaussian processes. *Geophysical Journal International*, *226*(3), 1705–1714. https://doi.org/10.1093/gji/ggab168

Langbein, J. (2004). Noise in two-color electronic distance meter measurements revisited. *Journal of Geophysical Research*, *109*(B4), B04406. https://doi.org/10.1029/2003JB002819

Langbein, J. (2012). Estimating rate uncertainty with maximum likelihood: Differences between power-law and flicker-random-walk models. *Journal of Geodesy*, *86*(9), 775–783. https://doi.org/10.1007/s00190-012-0556-5

Langbein, J., & Johnson, H. (1997). Correlated errors in geodetic time series: Implications for time-dependent deformation. *Journal of Geophysical Research*, *102*(B1), 591–603. https://doi.org/10.1029/96JB02945

Lanzi, C., Drouin, V., Sigmundsson, F., Geirsson, H., Hersir, G. P., Ágústsson, K., et al. (2023). Pressure increase at the magma-hydrothermal interface at Krafla caldera, North-Iceland, 2018–2020: Magmatic processes or hydrothermal changes? *Journal of Volcanology and Geothermal Research*, *440*, 107849. https://doi.org/10.1016/j.jvolgeores.2023.107849

Liu, F., Elliott, J. R., Ebmeier, S. K., Craig, T. J., Hooper, A., Novoa Lizama, C., & Delgado, F. (2023). First onset of unrest captured at Socompa: A recent geodetic survey at central Andean volcanoes in northern Chile. *Geophysical Research Letters*, *50*(10), e2022GL102480. https://doi.org/10.1029/2022GL102480

Mao, A., Harrison, C., & Dixon, T. H. (1999). Noise in GPS coordinate time series. *Journal of Geophysical Research*, *104*(B2), 2797–2816. https://doi.org/10.1029/1998JB900033

Marquart, G., & Jacoby, W. (1985). On the mechanism of magma injection and plate divergence during the Krafla Rifting Episode in NE Iceland. *Journal of Geophysical Research*, *90*(B12), 10178–10192. https://doi.org/10.1029/JB090iB12p10178

Metropolis, N., Rosenbluth, A. W., Rosenbluth, M. N., Teller, A. H., & Teller, E. (1953). Equation of state calculations by fast computing machines. *The Journal of Chemical Physics*, *21*(6), 1087–1092. https://doi.org/10.1063/1.1699114

Nikolaidis, R. (2002). *Observation of geodetic and seismic deformation with the global positioning system, (Doctoral dissertation)*. University of California. Retrieved from Scripps Orbit and Permanent Array Center Retrieved from http://sopac.ucsd.edu/input/processing/pubs/nikoThesis.pdf

Oelsmann, J., Passaro, M., Sánchez, L., Dettmering, D., Schwatke, C., & Seitz, F. (2022). Bayesian modelling of piecewise trends and discontinuities to improve the estimation of coastal vertical land motion. *Journal of Geodesy*, *96*(9), 62. https://doi.org/10.1007/s00190-022-01645-6

Olivare-Pulido, G., Teferle, F. N., & Hunegnaw, A. (2020). Markov chain Monte Carlo and the application to geodetic time series analysis. In J. P. Montillet & M. Bos (Eds.), *Geodetic time series analysis in Earth sciences*. Springer.

Olivares, G., & Teferle, F. N. (2013). A Bayesian Monte Carlo Markov chain method for parameter estimation of fractional differenced Gaussian processes. *IEEE Transactions on Signal Processing*, *61*(9), 2405–2412. https://doi.org/10.1109/TSP.2013.2245658

Parks, M. M., Heimisson, E. R., Sigmundsson, F., Hooper, A., Vogfjörd, K. S., Árnadóttir, T., et al. (2017). Evolution of deformation and stress changes during the caldera collapse and dyking at Bárdarbunga, 2014-2015: Implication for triggering of seismicity at nearby Tungnafellsjökull volcano. *Earth and Planetary Science Letters*, *462*, 212–223. https://doi.org/10.1016/j.epsl.2017.01.020

Qianqian, Z., & Qingming, Q. (2013). Bayesian methods for outliers detection in GNSS time series. *Journal of Geodesy*, *87*(7), 609–627. https://doi.org/10.1007/s00190-013-0640-5

Saemundsson, K. (1979). Outline of the geology of Iceland. *Jökull*, *29*(1), 7–28. https://doi.org/10.33799/jokull1979.29.007

Schuler, J., Pugh, D. J., Hauksson, E., White, R. S., Stock, J. M., & Brandsdóttir, B. (2016). Focal mechanisms and size distribution of earthquakes beneath the Krafla central volcano, NE Iceland. *Journal of Geophysical Research: Solid Earth*, *121*(7), 5152–5168. https://doi.org/10.1002/2016JB013213

Sigmundsson, F., Einarsson, P., Hjartardóttir, A. R., Drouin, V., Jónsdóttir, K., Árnadóttir, T., et al. (2020). Geodynamics of Iceland and the signatures of plate spreading. *Journal of Volcanology and Geothermal Research*, *391*, 106436. https://doi.org/10.1016/j.jvolgeores.2018.08.014

Sigmundsson, F., Hooper, A., Hreinsdóttir, S., Vogfjörd, K. S., Ófeigsson, B. G., Heimisson, E. R., et al. (2014). Segmented lateral dyke growth in a rifting event at Bárðarbunga volcanic system, Iceland. *Nature*, *517*(7533), 191–195. https://doi.org/10.1038/nature14111

Sigmundsson, F., Pinel, V., Grapenthin, R., Hooper, A., Halldórsson, S. A., Einarsson, P., et al. (2020). Unexpected large eruptions from buoyant magma bodies within viscoelastic crust. *Nature Communications*, *11*(1), 2403. https://doi.org/10.1038/s41467-020-16054-6

Tryggvason, E. (1989). Ground deformation in Askja, Iceland: Its source and possible relation to flow of the mantle plume. *Journal of Volcanology and Geothermal Research*, *39*(1), 61–67. https://doi.org/10.1016/0377-0273(89)90021-8

Vitti, A. (2012). Sigseg: A tool for the detection of position and velocity discontinuities in geodetic time-series. *GPS Solutions*, *16*(3), 405–410. https://doi.org/10.1007/s10291-012-0257-9

Wang, L., & Herring, T. (2019). Impact of estimating position offsets on the uncertainties of GNSS site velocity estimates. *Journal of Geophysical Research: Solid Earth*, *124*(12), 13452–13467. https://doi.org/10.1029/2019JB017705

Wang, X., Cheng, Y., Wu, S., & Zhang, K. (2016). An enhanced singular spectrum analysis method for constructing nonsecular model of GPS site movement. *Journal of Geophysical Research: Solid Earth*, *121*(3), 2193–2211. https://doi.org/10.1002/2015JB012573

Wessel, P., Luis, J. F., Uieda, L., Scharroo, R., Wobbe, F., Smith, W. H. F., & Tian, D. (2019). The generic mapping tools version 6. *Geochemistry, Geophysics, Geosystems*, *20*(11), 5556–5564. https://doi.org/10.1029/2019GC008515

Williams, S. D. P. (2003). The effect of coloured noise on the uncertainties of rates estimated from geodetic time series. *Journal of Geodesy*, *76*(9–10), 483–494. https://doi.org/10.1007/s00190-002-0283-4

Wright, T., Sigmundsson, F., Pagli, C., Belachew, M., Hamling, I. J., Brandsdóttir, B., et al. (2012). Geophysical constraints on the dynamics of spreading centres from rifting episodes on land. *Nature Geoscience*, *5*(4), 242–250. https://doi.org/10.1038/ngeo1428

Wu, D., Yan, H., & Yuan, S. (2018). L1 regularization for detecting offsets and trend change points in GNSS time series. *GPS Solutions*, *22*(3), 88. https://doi.org/10.1007/s10291-018-0756-4

Zhou, X., Yang, Y., Chen, H., Ouyang, W., & Fan, W. (2019). A modified Least Square harmonics estimation method and comparative analysis of established full periodicity models. *Earth and Space Science*, *6*(11), 2160–2179. https://doi.org/10.1029/2019EA000750

References From the Supporting Information

Altamimi, Z., Rebischung, P., Métivier, L., & Collilieux, X. (2016). ITRF2014: A new release of the international terrestrial reference frame modeling nonlinear station motions. *Journal of Geophysical Research: Solid Earth*, *121*(8), 6109–6131. https://doi.org/10.1002/2016JB013098

Boehm, J., Werl, B., & Schuh, H. (2006). Troposphere mapping functions for GPS and very long baseline interferometry from European centre for medium-range weather forecasts operational analysis data. *Journal of Geophysical Research*, *111*(B2), B02406. https://doi.org/10.1029/2005JB003629

Gazeaux, J., Williams, S., King, M., Bos, M., Dach, R., Deo, M., et al. (2013). Detecting offsets in GPS time series: First results from the detection of offsets in GPS experiment. *Journal of Geophysical Research: Solid Earth*, *118*(5), 2397–2407. https://doi.org/10.1002/jgrb.50152

Leys, C., Ley, C., Klein, O., Bernard, P., & Licata, L. (2013). Detecting outliers: Do not use standard deviation around the mean, use absolute deviation around the median. *Journal of Experimental Social Psychology*, *49*(4), 764–766. https://doi.org/10.1016/j.jesp.2013.03.013

Lyard, F., Lefevre, F., Letellier, T., & Francis, O. (2006). Modelling the global ocean tides: Modern insights from FES2004. *Ocean Dynamics*, *56*(5–6), 394–415. https://doi.org/10.1007/s10236-006-0086-x